Fidelity of the APHRODITE Dataset in Representation of Extreme Precipitation over Central Asia

Sheng Lai[1,2], Zuowei Xie*[2], Cholaw Bueh[2] and Yuanfa Gong[1]

[1] *College of Atmospheric Science, Chengdu University of Information Technology, Chengdu 610225, China*

[2] *International Center for Climate and Environment Sciences, Institute of Atmospheric Physics, Chinese Academy of Sciences, Beijing 100029, China*

ABSTRACT

Using rain-gauge-observation daily precipitation data from the Global Historical Climatology Network (V3.25) and the Chinese surface daily climate dataset (V3.0), this study investigates the fidelity of the AHPRODITE dataset in representing extreme precipitation, in terms of the extreme precipitation threshold value, occurrence number, probability of detection and extremal dependence index during the cool (October to April) and warm (May to September) seasons in Central Asia during 1961–1990. The distribution of extreme precipitation is characterized by large extreme precipitation threshold values and high occurrence numbers over the mountainous areas. The APHRODITE dataset is highly correlated with the gauge-observation precipitation data and can reproduce the spatial distributions of the extreme precipitation threshold value and total occurrence number. However, APHRODITE generally underestimates the extreme precipitation threshold values, while it overestimates the total numbers of extreme precipitation events, particularly over the mountainous areas. These biases can be attributed to the

*Corresponding author: Zuowei Xie
Email: xiezuowei@mail.iap.ac.cn

overestimation of light rainfall and the underestimation of heavy rainfall induced by the rainfall distribution-based interpolation. Such deficits are more evident for the warm season with respect to the cool season, and thus the biases are more pronounced in the warm season than in the cool season. The probability of detection and extremal dependence index reveal that APHRODITE has a good capability of detecting extreme precipitation, particularly in the cool season.

Key words: APHRODITE; extreme precipitation; Central Asia; Xinjiang; fidelity.

https://doi.org/10.1007/s00376-020-0098-3

Article Highlights:

- APHRODITE can reproduce the spatial distributions of the extreme precipitation threshold value and total occurrence number.
- APHRODITE underestimates the extreme precipitation threshold values and overestimates the total numbers of the extreme precipitation.
- The warm season features stronger shift of precipitation distribution "spectrum" to smaller amplitudes resulting in higher biases with respect to the cool season.

1. Introduction

Human-induced climate change has increased the occurrence and intensity of extreme weather and climate events that cause huge losses to human society and natural ecosystems (Trenberth et al., 2015). The arid and semi-arid regions—which are characterized by rare precipitation, strong evaporation and fragile natural ecosystems—are experiencing more drastic climate change compared with global climate change (Chen et al., 2013; Hulme, 1996; Lioubimtseva and Henebry, 2009). A flurry of new studies has shown a statistically significant warming trend of 0.6 ℃ per 10 yr for the arid region in northwestern China since the beginning of the twenty-first century, which is nearly five times the global warming trend of 0.13 °C per 10 yr (Wei and Wang, 2013; Hu et al., 2014). Furthermore, this evident warming trend is accompanied by increased precipitation and extreme rainfall events over the arid and semi-arid areas (Xie et al., 2018; Song and Bai, 2016; Donat et al., 2016; Chaney et al., 2014).

Central Asia extends from the Caspian Sea in the west to northwestern China, and includes of two of the world's nine arid and semi-arid regions (Hulme, 1996). Hu et al. (2017) and Chen et al. (2018) found that precipitation exhibits an increasing trend over Xinjiang, whereas a decreasing trend over five states in Central Asia. Extreme precipitation accounts for 41.9% of the annual precipitation in the Tianshan Mountains (Yang, 2003) and is therefore one of the key factors affecting the security of water resources (Eekhout et al., 2018) and the stability of fragile ecosystems (Pueppke et al., 2018; Holmgren et al., 2006) in Central Asia. Zhang et al. (2017) found that the frequency and intensity of extreme precipitation increased significantly during 1938–2005 over Central Asia. Extreme precipitation in Xinjiang also showed a significant increasing trend in both frequency and intensity (Yang, 2003; Qi et al., 2015; Li et al., 2015). Owing to the increasing trend of extreme precipitation and its dominant contribution to the annual precipitation, it is important to systematically investigate the daily extreme precipitation over Central Asia, including Xinjiang.

Given that Central Asia features a complicated topography and the predominant rainfall distribution over the mountains (Hu et al., 2016; Guo et al., 2017), a high-resolution gridded data or a large number of gauge-observation data is necessarily required to delineate extreme precipitation properties over Central Asia. However, the gauge-observation daily precipitation data from meteorological stations of the Global Historical Climatology Network Daily (GHCN-D) is sparse and has declined substantially since 1991 over Central Asia due to the collapse of the Soviet Union (Hu et al., 2016; Zhang et al., 2017). The Asian Precipitation - Highly-Resolved Observational Data Integration Towards Evaluation (APHRODITE) precipitation dataset is the only long-term (1950–2015) daily gridded precipitation dataset for Eurasia and is interpolated from gauge-observation data (Yatagai et al., 2012). Although the faithfulness of APHRODITE precipitation data has been noted for different regions of the world, the studies were primarily based on monthly mean (Yatagai et al., 2012), index-based (Villafuerte II and Matsumoto, 2015; Singh and Qin, 2019) comparisons, or the frequency of fixed precipitation values (Han and Zhou, 2010; He et al., 2019). We try to assess the daily extreme precipitation from the APHRODITE dataset with the gauge-observation data for the period over 1960-1990. Since the APHRODITE dataset incorporates most gauge-observation data, it is hard to find gauge-observation data independent from the APRHODITE dataset. Therefore, this study is an analysis of the assimilation technique rather than a validation of the APHRODITE dataset relative to an independent ground truth. We hope the result could provide some clues for the improvement of algorithms and some helpful information for scientists.

Previous studies have mainly focused on the faithfulness of gridded data in terms of error indices and precipitation hit bias. This study aims to evaluate daily extreme precipitation from the APHRODITE dataset over Central Asia, including Xinjiang, over the 30-base-year period of 1961–1990 in terms of the extreme precipitation threshold value and total number of extreme precipitation events. Their differences are explained on the basis of precipitation error. The overall performance of APHRODITE for extreme precipitation is given by the probability of detection (POD) and the extremal dependence index (EDI) (Ferro and Stephenson, 2011). The remainder of this paper is organized as follows. Section 2 describes the data and analysis methods. Section 3 reports the results. Section 4 provides a discussion followed by a summary of the results in section 5.

2. Data and Methods

2.1 Study Area

Figure 1 shows the location of the study area of Central Asia with topography features and the distribution of the meteorological stations. In this study, Central Asia encompasses five countries, namely Kazakhstan, Kyrgyzstan, Tajikistan, Turkmenistan and Uzbekistan, and Xinjiang province in northwestern China. Central Asia is geographically high in the east and low in the west. The topography mainly includes deserts, plains, hills and mountains. The average altitude of the Pamirs Plateau and Tianshan Mountains is above 4000 m. Three major rivers—the Syr Darya, the Amu Darya and the Ili rivers—originate from the mountainous regions and flow into the lowlands and basins in the west. The climate of Central Asia is characterized by a typical continental climate (Df/Ds) with annual precipitation ranging from 700 to 1200 mm in the mountainous areas, and semi-arid (BSk) and desert (BWk) climates with annual precipitation of about 150 mm in the lowlands and basins (Beck et al., 2018).

2.2 Data

2.2.1 Gauge-observation Precipitation Datasets

The observed precipitation data come from two rain-gauge-observation datasets, which are GHCN-D Version 3.25 and the dataset of daily climate data from Chinese meteorological stations for global exchange version 3.0. The GHCN-D V3.25 is an integrated database of daily climate summarized from land surface stations across the globe, which contains records from over 100,000 stations in 180 countries and territories. The data undergo a series of quality checks before they are collected into the GHCN-D database. However, the GHCN-D dataset includes only 18 meteorological stations in Xinjiang, which is less than the number of Chinese national meteorological stations. To incorporate more meteorological stations, we adopt daily precipitation data from the Chinese surface stations for global exchange version 3.0 provided by the China Meteorological Data Service Center (CMDC) (https://data.cma.cn/en/). After strict quality control by manually rechecking and rectifying all suspicious and incorrect data, this dataset is homogeneous and reliable with a correct data rate close to 100%.

Given the lack of gauge-observation precipitation data over Central Asia since 1991, we focus on the period from 1 January 1961 to 31 December 1990. Furthermore, we chose meteorological stations with data available for at least 90% of the total number of days during 1961–1990. With this criterion, we obtained a total of 253 meteorological stations within the five countries from the GHCN-D and 63 meteorological stations in the Xinjiang region from the CMDC (Figure 1). Figure 2 shows the percentage of the total number of days with available precipitation data in each year for the 316 meteorological stations. The average percentage of the total number of days with available precipitation data is 97.3%. Station numbers 51053 and above have a correct data rate of nearly 100%.

2.2.2 Gridded Precipitation Dataset

The APHRODITE project aims to provide long-term, high-resolution daily gridded precipitation and temperature datasets over Asia. The gridded precipitation dataset is interpolated from GTS-based data from gauge observations, data precompiled by other projects or organizations, such as other national hydrological and meteorological services, and data from individual collections. The interpolation of gauge-observation data to gridded data is applied to the ratio of daily precipitation to daily climatology using a Spheremap-type scheme, which considers daily-variation weighting based on the rainfall distribution. Considering the current study period of 1961–1990, we use the gridded daily precipitation over Russia/Northern Eurasia (APHRO_RU_V1101) from APHRODITE. The APHRO_RU_V1101 daily precipitation dataset is on a 0.25° × 0.25° latitude–longitude grid and covers northern Eurasia for the period 1951–2007. We also use the ratio of 0.05° grid box containing stations provided by this dataset.

Compared with the GTS analysis and the Global Precipitation Climatology Centre (GPCC) full archive product version 4 (Schneider et al., 2008), the APHRODITE precipitation data are more accurate over Central Asia and the mountainous areas as it uses more gauge-observation data. Furthermore, a considerable number of studies have used APHRODITE as a reference dataset for comparison or modeling. Readers are referred to Yatagai et al. (2012) for more information.

2.3 Method

2.3.1 Definition of Extreme Precipitation

Given the relatively large spatial variation of precipitation over Central Asia, we adopt percentile-based values rather than fixed absolute values to define the extreme precipitation threshold value for each station or grid point. In addition, considering the differences in the general circulation and precipitation phase between summer and winter, we separate each year into the boreal cool (October to April) and warm (May to September) seasons. The percentile-based extreme precipitation threshold value for each station or grid point is defined based on the following procedure:

(1) Daily precipitation data of 1.0 mm or more were sorted in an ascending order (X_1, X_2,...,X_q,...,X_n) for each station or grid point during the warm or cool seasons over 1961–1990.

(2) The value corresponding to percentile q is determined by:

$$X_q = X_{Ni} + r(X_{Ni+1} - X_{Ni}) \tag{1}$$

where

$$Ni1 = floor\left(q \times \left(n + \frac{1}{3}\right) + \frac{1}{3}\right) \tag{2}$$

$$r = q \times (n+1) - floor(q \times (n+1)) \tag{3}$$

n is the total number of days with precipitation of 1.0 mm or more for each station or grid point, and $floor(Y)$ is the largest integer less than or equal to Y. Compared with other quantile definitions, this definition is a median-unbiased estimator regardless of the distribution (Hyndman and Fan, 1996). Following Zhai and Pan (2003), the percentile q chosen here is 95%. Extreme precipitation at a station or grid point is identified if the daily precipitation is above the extreme precipitation threshold value. The extreme events are counted for each day and each gauge-observation station or grid point. Therefore, an extreme event is referred to a station or grid point and there could be several extreme events on a single day.

Noting the complicated interpolation of APHRODITE, we simply pick up the grid point nearest to the gauge-observation station to avoid additional bias induced by our interpolation (Qi et al., 2015; Hu et al., 2018). The average distance between each gauge-observation station and its nearest grid point of APHRODITE is 9.1 km. For the extreme precipitation to be more comparable between two datasets, daily precipitation of an APHRODITE grid point is removed if there is a missing value in its nearest gauge-observation station.

Since this study evaluates the APHRODITE data according to the gauge-observation data, we consider the grid point is identical to its nearest gauge-observation station assuming that the distance between them could be negligible for the extreme precipitation detection. Figures 4 and 5 are generated by interpolating the gauge-observation and the APHRODITE values into a 0.07×0.15 latitude/longitude grid using the geographic information of the gauge-observation station regardless of the APRHODITE gird point information. The interpolation mothed used here is radial basis function interpolation (UCAR Unidata/MetPy: https://unidata.github.io/MetPy/latest/examples/gridding/Point_Interpolation.html). Similarly, such interpolation is applied to the biases between the gauge-observation values and the APHRODITE values, POD and EDI.

2.3.2 Statistical Evaluation Metrics

To assess the extreme precipitation detection ability of the APHRODITE dataset, we use the POD and the EDI to evaluate the fidelity of the APHRODITE dataset. The (POD), false detection ratio (FDR) and EDI are calculated based on a contingency table as shown in Table 1 and defined as:

$$POD = \frac{H}{H + M} \tag{5}$$

$$FDR = \frac{F}{F + N} \tag{6}$$

$$EDI = \frac{log\,FDR - log\,POD}{log\,FDR + log\,POD} \tag{7}$$

where the number of hits of extreme precipitation (*H*), false detections (*F*) and correct negatives (*N*) are defined in Table 1.

The POD represents the ratio of the number of extreme precipitation events detected correctly by the APHRODITE dataset; the FDR denotes the proportion of the extreme precipitation events in which the APHRODITE dataset identifies extreme precipitation when the gauge-observation station does not. Compared with the POD and FDR, the EDI is base-rate independent, asymptotically equitable and non-degenerating (Ferro and Stephenson, 2011). The POD and FDR range from 0 to 1, and the EDI falls between −1 and 1. For a perfect detection, the POD and EDI is 1, while the FDR is 0.

3. Results

3.1 Spatial Distribution of Extreme Precipitation

In order to describe the spatial characteristics of extreme precipitation events, we compute probability density functions (PDF) distributions of extreme precipitation station numbers in each day for the cool and warm seasons, which are shown in Figure 3. Daily extreme precipitation station numbers are primarily between 1 and 3 (i.e., below 1% of total number of stations) with percentages of 59.16% and 70.20% for the cool and warm seasons, respectively. The result suggests that the extreme precipitation events over Central Asia are mainly very localized. In comparison with the cool season, the PDF distribution of the warm season shifts right substantially to the bins with small numbers of stations, indicating more localized extreme precipitation events in the warm season.

Figure 4 shows the spatial distribution of extreme precipitation threshold values during the boreal cool and warm seasons for the observations and the APHRODITE data. In general, the maxima of extreme precipitation threshold values are distributed along the mountains in Central Asia in both the observations and the APHRODITE data. In the cool season, the amplitudes of extreme precipitation threshold values are above 6 mm d^{-1} and reach up to 24 mm d^{-1} (Fig. 4a). The maxima are situated to the north of the Plateau of Iran, the Hindu Kush Mountains, Pamir, the western Tianshan Mountains and Kazakhskiy Melkosopochnik. The spatial distribution of APHRODITE basically resembles that of the observations but with smaller threshold values (Fig. 4b). Large biases of APHRODITE with respect to observations mainly occur over the north of the Plateau of Iran, Kazakhskiy Melkosopochnik and Xinjiang (Fig. 4c). In contrast, the warm season features larger extreme precipitation threshold values and broader maxima areas (Fig. 4d). The maximum over Pamir extends northwestward to the Aral Sea and additional maxima are seen over the east to the Caspian Sea and the eastern Tianshan Mountains. Although the spatial distribution of APHRODITE concurs with the observations, the negative biases in the warm season are nearly double their cool season counterparts (Figs. 4e and f). This underestimation of daily extreme precipitation threshold values agrees with the underestimation of monthly and annual precipitation of GPCC, Climate Research Unit (CRU) and Willmott and Matsuura (WM) datasets (Hu et al., 2018). Unlike the monthly and annual precipitation biases, which are the largest over the mountains, the biases in daily extreme precipitation threshold values are smaller over the mountains than the lowlands.

Figure 5 shows the spatial distribution of the total numbers of extreme precipitation events during the cool and warm seasons over 1961-1990 for the observations and the APHRODITE data. Similar to the distribution of extreme precipitation threshold values, extreme precipitation primarily occurs over the mountains. In contrast, the biases mainly occur over the main regions of extreme precipitation. The cool season features a region of abnormally high numbers of extreme precipitation (up to 121 days) extending from the north of the Hindu Kush Mountains via Pamir to the Altai Mountains with two low centers to its east and west (Fig. 5a). In addition, moderately high numbers of extreme precipitation are observed over Kazakhskiy Melkosopochnik and to the south of the Ural Mountains. The distribution of total numbers of extreme precipitation in the APRHODITE data is consistent with the observations but with a larger magnitude (Fig. 5b). The overestimation regions coincide with the maxima of extreme precipitation occurrence and 29.4% of the total number of grid points have biases above 5 days (Fig. 5c). In the warm season, the distribution of extreme precipitation occurrence numbers is more regional and more northward than the cool season counterparts (Fig. 5d). The maxima are confined to the Tianshan Mountains and the northern border of Kazakhstan. Furthermore, there is a broader small number of extreme precipitation over the Turan Plain. Although the distribution of APHRODITE resembles that of the observations, the biases in the warm season are greater than those in the cool season (Fig. 5f). The percentage of grid points with biases beyond 5 days increases to 38.6%.

Figure 6 shows time series of the total numbers of extreme precipitation events in each month derived from the 316 gauge-observation stations and APHRODITE grid points for the cool and warm seasons. The time series of APRHODITE are basically consistent with those of gauge observation with correlation coefficients of 0.98 and 0.95 at 99.9% confidence level for the cool and warm seasons, respectively. Considering the cool season, APHRODITE tends to overestimate the large numbers of extreme precipitation events, while underestimate the small numbers of events (Fig. 6a). In contrast, the warm season features more evident overpopulation of both the small and large numbers of extreme precipitation events (Fig. 6b).

3.2 Possible Causes of the Bias

To illustrate the potential causative factors of the aforementioned lower threshold values and higher occurrence frequencies of extreme precipitation in APHRODITE relative to the observations, we calculate the PDFs and total number of wet days (> 1 mm d^{-1}) from the two datasets. Figure 7 shows scatterplots and PDFs of the observation and APHRODITE precipitation data during the cool and warm seasons. The APHRODITE daily precipitation is highly correlated with the gauge-observation precipitation, which is significant at the 99% confidence level ($p < 0.01$). The scatterplots show that these two datasets concentrate along their liner regression line, particularly in the cool season (Figs. 7a and b). The coefficients of linear regression for the cool and warm seasons are 0.79 and 0.64, respectively, which indicates that APHRODITE has a tendency to underestimate the precipitation amplitude. However, the regression constants are positive, suggesting more small precipitation values in APRHODITE than in the observations. As seen from Figs. 7c and d, APHRODITE overestimates the precipitation between 1 mm d^{-1} and 4 mm d^{-1}, particularly in the warm season. This suggests that the precipitation distribution "spectrum" shifts to smaller amplitudes. It can be concluded from the percentile-based extreme definition that the overestimation of light precipitation and underestimation of moderate and heavy precipitation both contribute to the smaller extreme precipitation threshold values of APHRODITE with respect to the observations.

Figure 8 shows the spatial distribution of the biases in the total number of the wet days (>1 mm d^{-1}) between APHRODITE and the observations. The total number of the wet days is generally larger in AHPRODITE, ranging from 20 to 350 days. The spatial distributions strongly resemble the biases of the total numbers of extreme precipitation (Figs. 5c and f). As the interpolation of APHRODITE precipitation is based on the rainfall distribution, the precipitation at gauge-observation stations adjacent to a grid point of APHRODITE could be carried into the grid point even though its nearest gauge-observation station does not have rainfall. However, such interpolation could overestimate the precipitation amplitude at a grid point if there is a precipitation maximum at its nearest gauge-observation station. These two deficits tend to be more pronounced over the regions with larger annual precipitation (i.e., the larger extreme precipitation threshold values), resulting in more evident overestimation of extreme precipitation.

Considering the cool season, the average precipitation and standard deviation are 4.4 mm d^{-1} and 5.53, respectively. In comparison with the cool season, the warm season features more precipitation (5.5 mm d^{-1}) with larger variance (6.67). The interpolation induces more evident shift of precipitation distribution "spectrum" to smaller amplitudes for the warm season with respect to the cool season (Fig. 7), which result in smaller extreme threshold values and stronger overpopulation of extreme precipitation relative to the gauge observation. Therefore, the biases are much higher in the warm season than those in the cool season.

3.3 Fidelity of Representation Extreme Precipitation

Figure 9 shows the spatial distribution of the POD of APHRODITE extreme precipitation in Central Asia. In the cool season, the POD values are generally above 0.70 over most parts of Central Asia except Kazakhskiy Melkosopochnik and the Tianshan Mountains in Xinjiang (Fig. 9a). The mean POD in Central Asia is 0.70, which suggests that 70% of the observed extreme precipitation is captured correctly by APHRODTE. Despite overestimating the number of extreme precipitation events over the mountains (Figs. 5c and f), a maximum above 0.85 is seen over Pamir. As the POD depends on the total number of extreme precipitation events in the observations, the overestimation of extreme precipitation events increases the likelihood of a high POD.

Similar to the aforementioned larger biases in the warm season, the warm season has smaller POD values than the cool season with a mean value of 0.65 (Fig. 9b). There are additional minima in the Turan Lowland (0.53) and the Tarim Basin (0.48), which overlap with small threshold values and low number of extreme precipitation events (Figs. 4f and 5f). High PODs corresponding to overestimated extreme precipitation and a low POD corresponding to small number of extreme precipitation events suggests that the POD depends on the total number of extreme precipitation events.

Figure 10 shows the spatial distribution of the EDI of extreme precipitation for APHRODITE during the cool and warm seasons. Compared with the POD, the EDI is more comparable between the low and high numbers of extreme precipitation events. The amplitudes of the EDI are obviously larger than the POD. In the cool and warm seasons, 84.2% and 64.6% of grid points have EDI scores above 0.8, respectively. Three minima remain over northern Kazakhstan and central Xinjiang. In general, the identification of extreme precipitation in APHRODITE can be regarded as considerably reliable.

As it can be seen from Fig. 1, there are some stations within a single grid box. To quantify the impact of the number of stations included in a single grid box, we compute the averages of the extreme precipitation biases, POD and EDI stratified by different number of stations within each of 316 grid boxes. The grid boxes mainly include 1 and 2 gauge-observation stations, which are 191 and 110, respectively. Besides, 13 grid boxes encompass 3 stations, while only 2 grid boxes include 5 stations. Table 2 shows the averages of extreme precipitation biases, POD and EDI stratified by 1, 2, 3 and 5 stations within a grid box. As it will be subsequently shown in the discussions, there are two stations not incorporated to APHRODITE and two stations with 5-year anomalous values, where the APHRODITE grid points exhibit relatively low performances. These four stations are only related to four grid boxes that include 3 stations. To be more comparable, we have removed these four stations and grid points for the grid box with 3 stations. There is an overall improvement of APHRODITE in representing extreme precipitation if the grid box incorporates 2 and 3 gauge-observation stations. Although the grid boxes with 5 stations have some improvements in POD and EDI with respect to those with 1 station, they exhibit an overall degradation compared to those with 2 and 3 stations. Such degradation could possibly be attributed to the impact of topography since these two grid boxes are both in the Trans-Ili Alatau Mountains with altitudes of 3185 m and 3966 m, respectively.

4. Discussions

It is noted that station numbers 36335, 51581 and 51655 (marked in Fig. 8a) have the lowest POD and EDI in the cool season. By checking the ratio of the 0.05° grid box containing stations provided by APHRODITE, we confirm that the APHRODITE dataset does not incorporate station numbers 51581 and 51655 in Xinjiang and station number 36335 in Kazakhskiy Melkosopochnik before 1966 in the interpolation. Apparently, owing to the absence of station numbers 51581 and 51655, their nearest grid points in APHRODITE fail to identify extreme precipitation.

We compare the gauge-observation precipitation of station number 36335 with the precipitation of its nearest grid point in APHRODITE in the warm season, which is shown in Figure 9. Although the number of extreme precipitation events is comparable between the two datasets, the extreme precipitation events do not exactly overlap with each other. The observational data show that extreme precipitation dominates during 1961–1965. In APRHODITE, this station is ruled out for this period after a series of quality control checks conducted by the APRHODITE gridding algorithm. As such, the predominant extreme precipitation events in the observations during 1961–1965 are absent in APHRODITE. As a result, the extreme precipitation threshold value dramatically declines from 38.2 mm d^{-1} for the observations to 12.1 mm d^{-1} for APRHODITE, resulting in more extreme precipitation since 1966 in the APRHODITE dataset. Therefore, station number 36335 has smaller values for both the POD and EDI. Similarly, the quality control processes of APHRODITE also rule out some of the extreme precipitation in the gauge observations, particularly in the desert areas, which results in relatively lower POD and EDI scores and higher negative biases of the threshold in the Turan Lowland and the Tarim Basin. We have checked carefully the other 315 stations, and there is another station No. 35582 similar to No. 36335.

Figure 10 shows the distribution of the distance between each observation station and its nearest grid point in APHRODITE. The distance shows a normal distribution with mean value of 9.1 km and a standard deviation of 3.6. The magnitude of the distance ranges between 1.1 km and 16.7 km. APHRODITE uses a modified distance-weighting interpolation method (Yatagai et al., 2012, 2018), which partially contributes to underestimation of precipitation and extreme precipitation extreme values. As we mainly focus on the representation of extreme precipitation rather than the precipitation errors, we assume that such a distance is negligible for the detection of extreme precipitation.

The number of extreme precipitation days is not comparable between the cool and warm seasons, which are 212*30 and 153*30, respectively. Strictly speaking, we should not directly compare the distribution of extreme precipitation between two seasons. However, this study compares the distribution of extreme precipitation in the warm season with that in the cool season to highlight the signatures of extreme precipitation and make the study more concise.

5. Conclusions

Using gauge-observation data, this study examines the fidelity of the APHRODITE dataset in representing extreme precipitation over Central Asia, which includes the conventional five countries and Xinjiang province in China, in terms of the extreme precipitation threshold value, the total number of extreme precipitation events, POD and EDI during the cool and warm seasons during 1961–1990.

The APHRODITE dataset is highly correlated with the gauge-observation precipitation data and can reproduce the spatial distributions of the extreme precipitation threshold value and occurrence number. For the cool season, the maxima of the extreme precipitation threshold value and occurrence number reside over the mountainous areas, such as the Hindu Kush Mountains, Pamir, the western Tianshan Mountains and Kazakhskiy Melkosopochnik. APHRODITE tends to underestimate the extreme precipitation threshold value, particularly over the regions with moderate threshold values. In contrast, APHRODITE overestimates extreme precipitation over the regions with greater threshold values. Considering the temporal feature, APRHODITE is basically consistent with gauge observation with an overall overpopulation, particularly during the time with large numbers of extreme precipitation events. The distribution-based interpolation of precipitation results in APHRODTE overestimating light rainfall and underestimating heavy rainfall. Therefore, APHRODITE underestimates the extreme precipitation threshold value and overestimates the total number of extreme precipitation events, particularly over the mountainous areas. Since more powerful shift of precipitation distribution “spectrum” to smaller amplitudes for the warm season with respect to the cool season, the biases are more evident in the warm season than the cool season.

The POD and EDI reveal that APHRODITE has a fairly good capability of detecting extreme precipitation, particularly in the cool season. The number of sampling grid points with POD values above 0.7 account for 79.7% of the grid points in the cool season and 60.7% in the warm season, while grid points with EDI values above 0.8 account for 84.2% and 64.6% of the grid points in the cool and warm seasons, respectively.

This study primarily focused on the representation of extreme precipitation in APHRODITE during 1961–1990 and interpreted the biases from the perspective of the precipitation distribution. The interannual and interdecadal variabilities of extreme precipitation and the corresponding large-scale meteorological patterns remain to be unexplored. To address these questions, our future study will extend the study period to 2015 to investigate the temporal variability of extreme precipitation on the basis of the current extreme precipitation threshold value as well as the underlying physical mechanisms using the APHRODTE dataset with the satellite precipitation data instead of gauge observation data. Based on our finding, it is appropriate to perform the extreme analysis with APHRODITE to the places that incorporates gauge-observation data. Extremes over places without incorporating gauge observation should be examined carefully with atmospheric circulations. The total number of gauge-observations stations over Central Asia experienced two drastic declines in 1991 and 2006, respectively, which is the same situation for APHRODITE (Yatagai et al., 2012, 2018). It is unrealistic to conduct the extreme analysis over Central Asia since 2007 using the gauge-observation data. Therefore, it would be better to use the APHRODITE dataset with the satellite precipitation data that calibrated with the APRHRODITE data over their overlap years, taking 1998-2004 for example (Yatagai et al., 2014).

Acknowledgments. The authors are grateful to two anonymous reviewers for their valuable comments and suggestions. This research was funded by National Key Research and Development Program of China (2018YFC1507101) and National Natural Science Foundation of China (41861144014, 41875078 and 41630424). We acknowledge the Hirosaki University for providing the APHRODITE precipitation data (http://aphrodite.st.hirosaki-u.ac.jp/download/). We thank the China Meteorological Data Service Center (CMDC) for providing the Chinese Surface Daily Climate Dataset (V3.0) (https://data.cma.cn/en/?r=data/detail&dataCode=SURF_CLI_CHN_MUL_DAY_CES_V3.0) and the National Oceanic and Atmospheric Administration, National Centers for Environmental Information (NOAA/NCEI) for providing the Global Historical Climatology Network Daily Dataset (V3.25) (Menne et al., 2012). We convey our gratitude to the contributors of the SciPy ecosystem (Virtanen et al., 2020), which was used for data analysis and visualization.

REFERENCES

Beck, H. E., N. E. Zimmermann, T. R. McVicar, N. Vergopolan, A. Berg, and E. F. Wood, 2018: Present and future Köppen-Geiger climate classification maps at 1-km resolution. *Scientific Data*, **5**, 180214.

Chaney, N., J. Sheffield, G. Villarini, and E. Wood, 2014: Development of a high-resolution gridded daily meteorological dataset over sub-Saharan Africa: spatial analysis of trends in climate extremes. *Journal of Climate*, **27**, 5815–5835.

Chen, X., F.Q. Jiang, Y.J. Wang, Y.M. Li, R.J. Hu, 2013: Characteristics of the eco-geographical pattern in arid land of Central Asia. *Arid Zone Res.*, **30**(3), 385–390.

Chen, X., S. Wang, Z. Hu, Q. Zhou, and Q. Hu, 2018: Spatiotemporal characteristics of seasonal precipitation and their relationships with ENSO in Central Asia during 1901-2013, *Journal of Geographical Sciences*, **28**, 1341–1368.

Donat, M. G., A. L. Lowry, L. V. Alexander, P. A. O’Gorman, and N. Maher, 2016: More extreme precipitation in the world’s dry and wet regions. *Nature Climate Change*, **6**, 508–513.

Eekhout, J., J. Hunink, W. Terink, and J. de Vente, 2018: Why increased extreme precipitation under climate change negatively affects water security. *Hydrology and Earth System Sciences*, **22**, 5935–5946.

Ferro, C., and D. Stephenson, 2011: Extremal dependence indices: improved verification measures for deterministic forecasts of rare binary events. *Weather and Forecasting*, **26**(5), 699–713.

Guo, H., A. Bao, F. Ndayisaba, T. Liu, A. Kurban, and P. De Maeyer, 2017: Systematical evaluation of satellite precipitation estimates over Central Asia using an improved error-component procedure. *Journal of Geophysical Research: Atmospheres*, **122**, 10906–10927.

Holmgren, M., and Coauthors, 2006: Extreme climatic events shape arid and semiarid ecosystems. *Frontiers in Ecology and the Environment*, **4**, 87–95.

Hu, Z., Q. Hu, C. Zhang, X. Chen, and Q. Li, 2016: Evaluation of reanalysis, spatially interpolated and satellite remotely sensed precipitation data sets in central Asia. *Journal of Geophysical Research: Atmospheres*, **121**(10), 5648–5663.

Hu, Z., Q. Zhou, X. Chen, J. Li, Q. Li, D. Chen, W. Liu, and G. Yin, 2018: Evaluation of three global gridded precipitation data sets in central Asia based on rain gauge observations. *International Journal of Climatology*, **38**(9), 3475–3493.

Hu, Z., C. Zhang, Q. Hu, and H. Tian, 2014: Temperature changes in Central Asia from 1979 to 2011 based on multiple datasets. *Journal of Climate*, **27**(3), 1143–1167.

Hu, Z., Q. Zhou, X. Chen, C. Qian, S. Wang, and J. Li, 2017: Variations and changes of annual precipitation in Central Asia over the last century. *International Journal of Climatology*, **37**,157–170.

Hulme, M., 1996: Recent climatic change in the world's drylands. *Geophysical Research Letters*, **23**(1), 61–64.

Hyndman, R., and Y. Fan, 1996: Sample quantiles in statistical packages. *The American Statistician*, **50**, 361–365.

Kulkarni, A., S. Patwardhan, K. K. Kumar, K. Ashok, and R. Krishnan, 2013: Projected climate change in the Hindu Kush–Himalayan region by using the high-resolution regional climate model PRECIS. *Mountain Research and Development*, **33**, 142–151, 110.

Li, J. X., C. L. Du, S. F. Du, J. Zhao, and C. C. Xu, 2015: Temporal-spatial variation and trend prediction of extreme precipitation events in Xinjiang. *Arid Zone Res.*, **32**(6), 1103–1112. (in Chinese with English abstract)

Lioubimtseva, E., and G. M. Henebry, 2009: Climate and environmental change in arid Central Asia: Impacts, vulnerability, and adaptations. *Journal of Arid Environments*, **73**(11), 963–977.

Menne, M., I. Durre, R. Vose, B. Gleason, and T. Houston, 2012: An overview of the global historical climatology network-daily database. *Journal of Atmospheric and Oceanic Technology*, **29**(7), 897–910.

Pueppke, S., S. Nurtazin, N. Graham, and J. Qi, 2018: Central Asia’s Ili river ecosystem as a wicked problem: unraveling complex interrelationships at the interface of water, energy, and food. *Water*, **10**, 541.

Qi, Y., H. Y. Chen, S. B. Fang, and W. G. Yu, 2015: Variation characteristics of extreme climate events in northwest china during 1961-2010. *Journal of Arid Meteorology*, **33**(6), 72–78. (in Chinese with English abstract)

Schneider, U., T. Fuchs, A. Meyer-Christoffer, and B. Rudolf, 2008: Global precipitation analysis products of the GPCC. Global Precipitation Climatology Centre (GPCC), DWD, 12 pp.

Singh, V., and X. Qin, 2019: Data assimilation for constructing long-term gridded daily rainfall time series over Southeast Asia. *Climate Dynamics*, **53**, 3289–3313.

Song, S., and J. Bai, 2016: Increasing Winter Precipitation over Arid Central Asia under Global Warming. *Atmosphere*, **7**, 139.

Trenberth, K. E., J. T. Fasullo, and T. G. Shepherd, 2015: Attribution of climate extreme events. *Nature Climate Change*, **5**, 725–730.

Villafuerte II, M. Q. V., and J. Matsumoto, 2015: Significant influences of global mean temperature and ENSO on extreme rainfall in Southeast Asia. *Journal of Climate*, **28**, 1905–1919.

Virtanen, P., and Coauthors, 2020: SciPy 1.0: fundamental algorithms for scientific computing in Python. *Nature Methods*, **17**, 261–272.

Wei, K., and L. Wang, 2013: Reexamination of the aridity conditions in arid northwestern China for the last decade. *Journal of Climate*, **26**(23), 9594–9602.

Xie, Z., Y. Zhou, and L. Yang, 2018: Review of study on precipitation in Xinjiang. *Torrential Rain & Disasters*, **37**(3), 204–212

Yang, L. M., 2003: Climate change of extreme precipitation in Xinjiang. *Acta Geographica Sinica*, **58**(4), 577-583. (in Chinese with English abstract)

Yatagai, A., K. Kamiguchi, O. Arakawa, A. Hamada, N. Yasutomi, and A. Kitoh, 2012: APHRODITE: Constructing a long-term daily gridded precipitation dataset for Asia based on a dense network of rain gauges. *Bulletin of the American Meteorological Society*, **93**(9), 1401–1415.

Yatagai, A., M. Maeda, M. Masuda, N. Suetou, N. Yasutomi, and S. Khadgarai, 2018: Asian precipitation – highly resolved observational data integration towards evaluation of extreme events (APHRODITE-2). IPSJ Tohoku Branch SIG Technical Report, **9**, A2-2. (in Japanese with English abstract)

Yatagai, A., T. N. Krishnamurti, V. Kumar, A. K. Mishra, and A. Simon, 2014: Use of APHRODITE rain gauge–based precipitation and TRMM 3B43 products for improving asian monsoon seasonal precipitation forecasts by the superensemble method. *Journal of Climate*, **27**, 1062–1069.

Zhai, P., and X. Pan, 2003: Changes in extreme temperature and precipitation over northern China during the second half of the 20th Century. *Acta Geographica Sinica*, **58**(Supplement), 1–10. (in Chinese with English abstract)

Zhang, M., Y. Chen, Y. Shen, and Y. Li, 2017: Changes of precipitation extremes in arid Central Asia. *Quaternary International*, **436**, 16–27.

Table 1. The contingency table of extreme precipitation detected by the APHRODITE dataset.

	Event observed	**Nonevent observed**	**Total**
Detected	H	F	H+F
Non-detected	M	N	M+N
Total	H+M	F+N	n

Table 2. The average biases of extreme threshold values (Δp95) and total number of extreme precipitation events (ΔEvents), POD and EDI stratified by the number of stations within a grid box for the cool and warm seasons.

Number of stations	Δp95		ΔEvents		POD		EDI	
	Cool	Warm	Cool	Warm	Cool	Warm	Cool	Warm
1	-2.93	-5.98	4.13	5.83	0.74	0.68	0.84	0.78
2	-2.10	-5.24	4.20	4.74	0.80	0.76	0.89	0.86
3	-1.28	-3.93	4.42	6.83	0.79	0.78	0.89	0.88
5	-3.34	-4.60	1.50	7.00	0.79	0.72	0.90	0.85

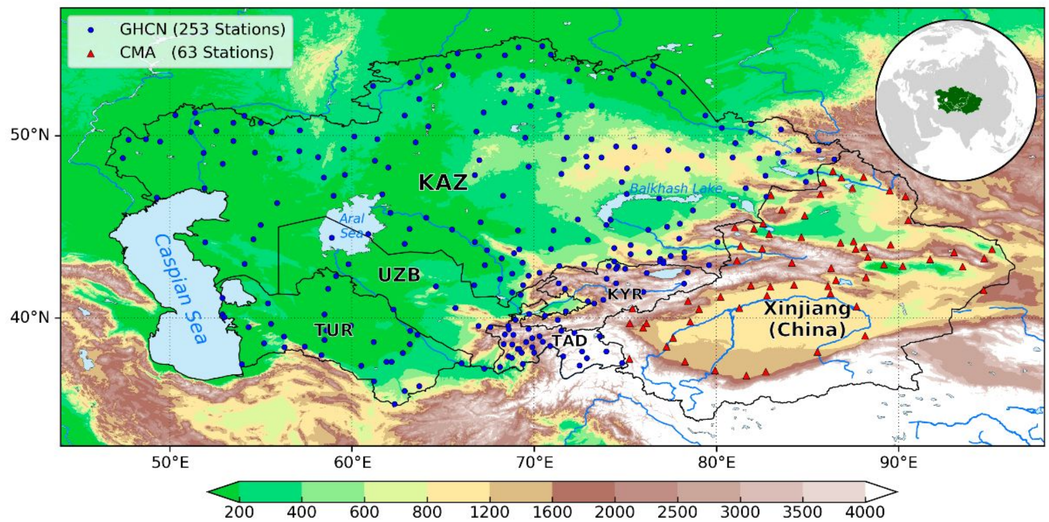

Fig. 1. Topography features and the distribution of the meteorological stations in Central Asia. Colored shading indicates the topography (units: m). Blue lines indicate the major rivers. KAZ, Kazakhstan; TAD, Tajikistan; TUR, Turkmenistan; KYR, Kyrgyzstan; UZB, Uzbekistan; Xinjiang, Xinjiang Uygur Autonomous Region of China.

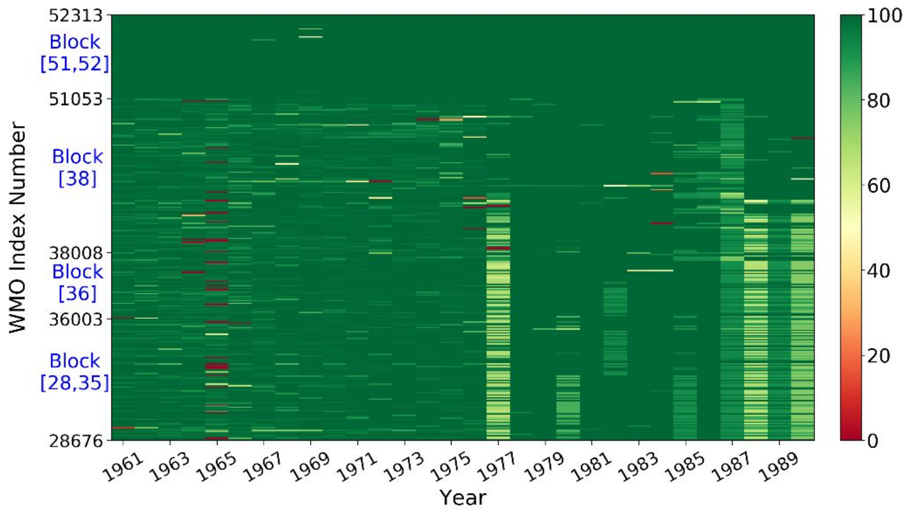

Fig. 2. The percentage of total number of days with available precipitation data in each year for 316 gauge-observation stations in Central Asia over 1961-1990.

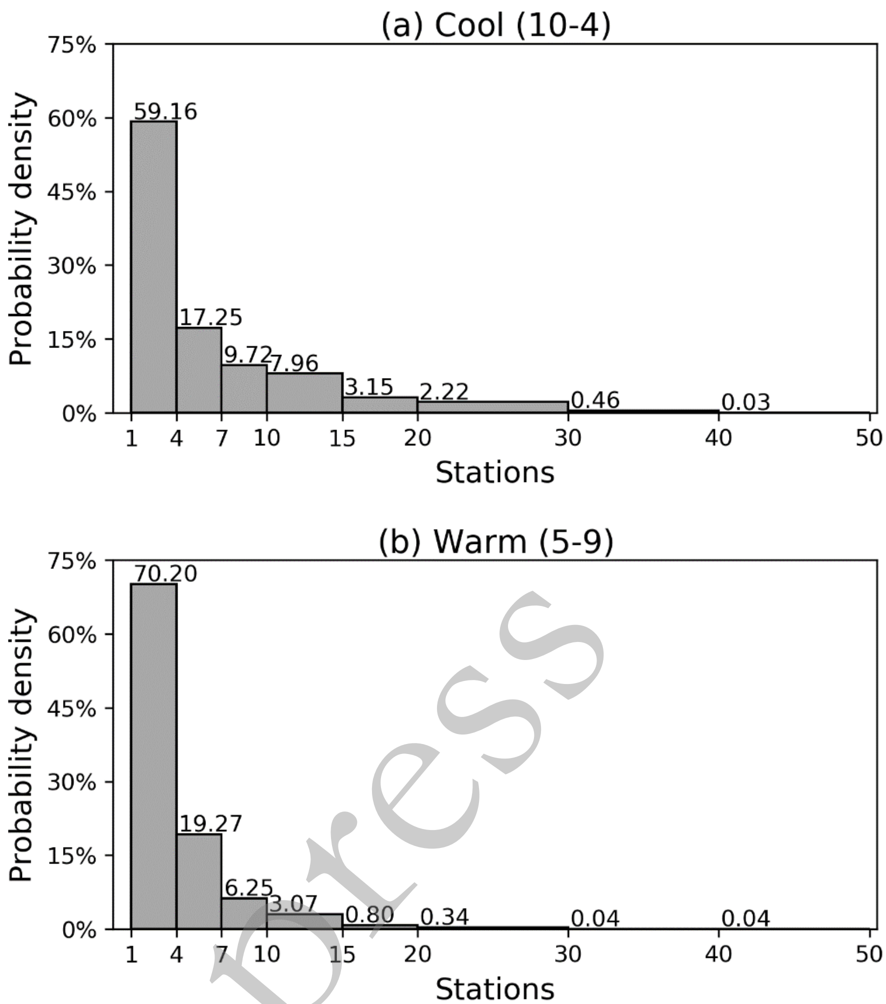

Fig. 3. PDF of extreme precipitation station numbers in each day for the (a) cool and (b) warm seasons.

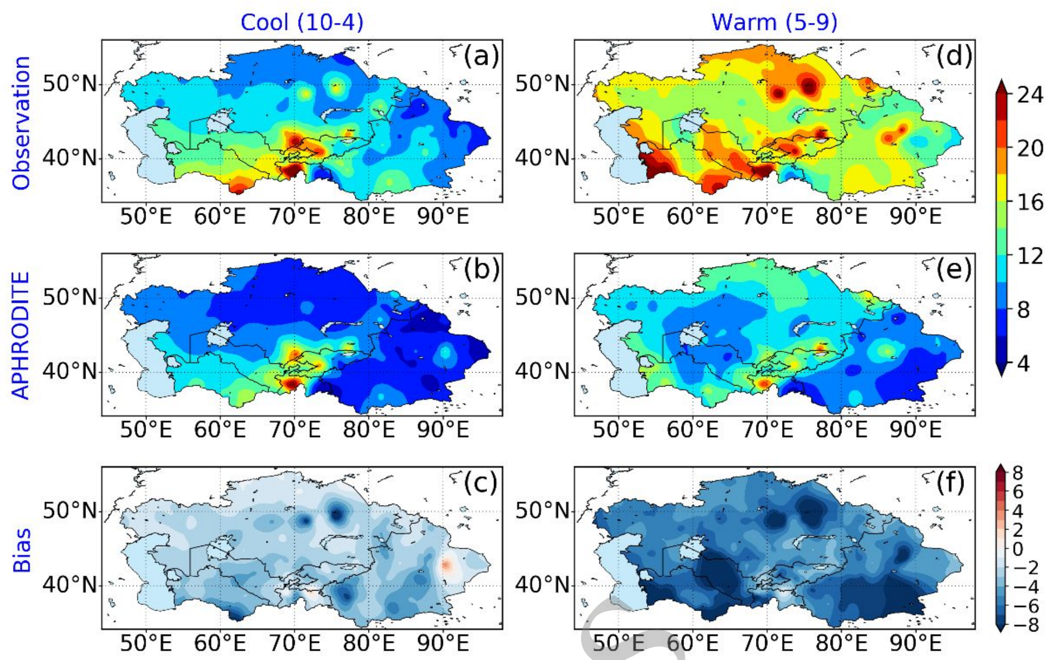

Fig. 4. The spatial distribution of extreme precipitation threshold values (units: mm d^{-1}) in the boreal cool season for (a) observations and (b) APHRODITE and (c) the bias between (b) and (a). (d)–(f) as for (a)–(c), but for the warm season.

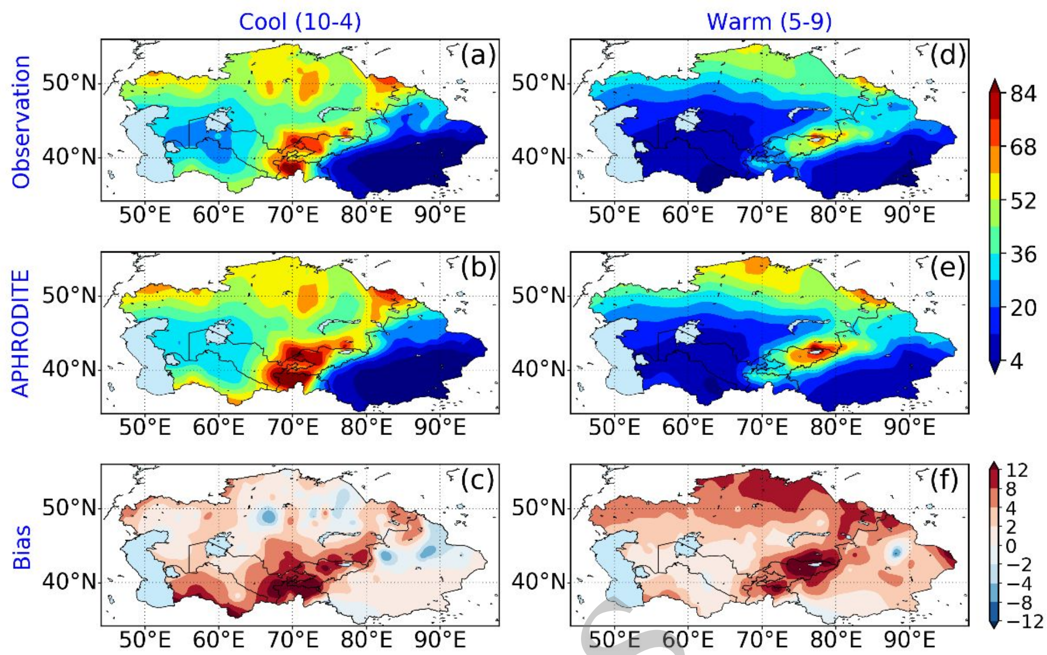

Fig. 5. As in Fig. 4, but for the total numbers of extreme precipitation events over 1961-1990.

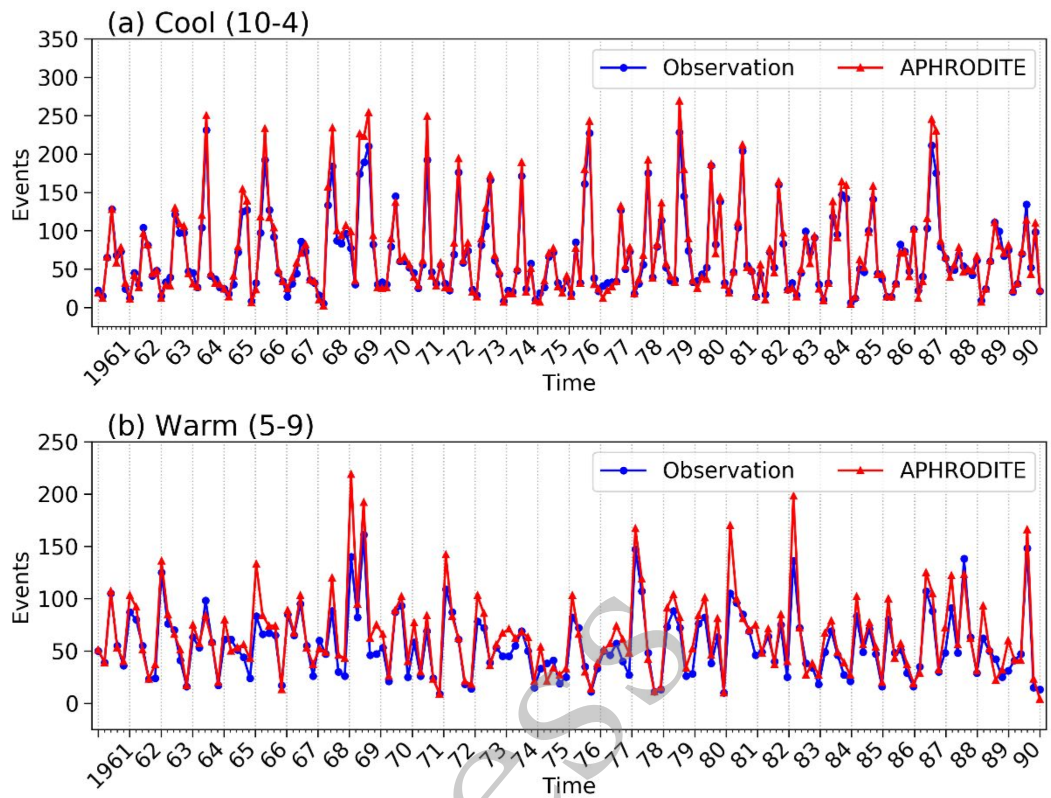

Fig. 6. Time series of the total numbers of extreme precipitation events in each month derived from the 316 gauge-observation stations (blue) and APHRODITE grid points (red) for the (a) cool and (b) warm seasons.

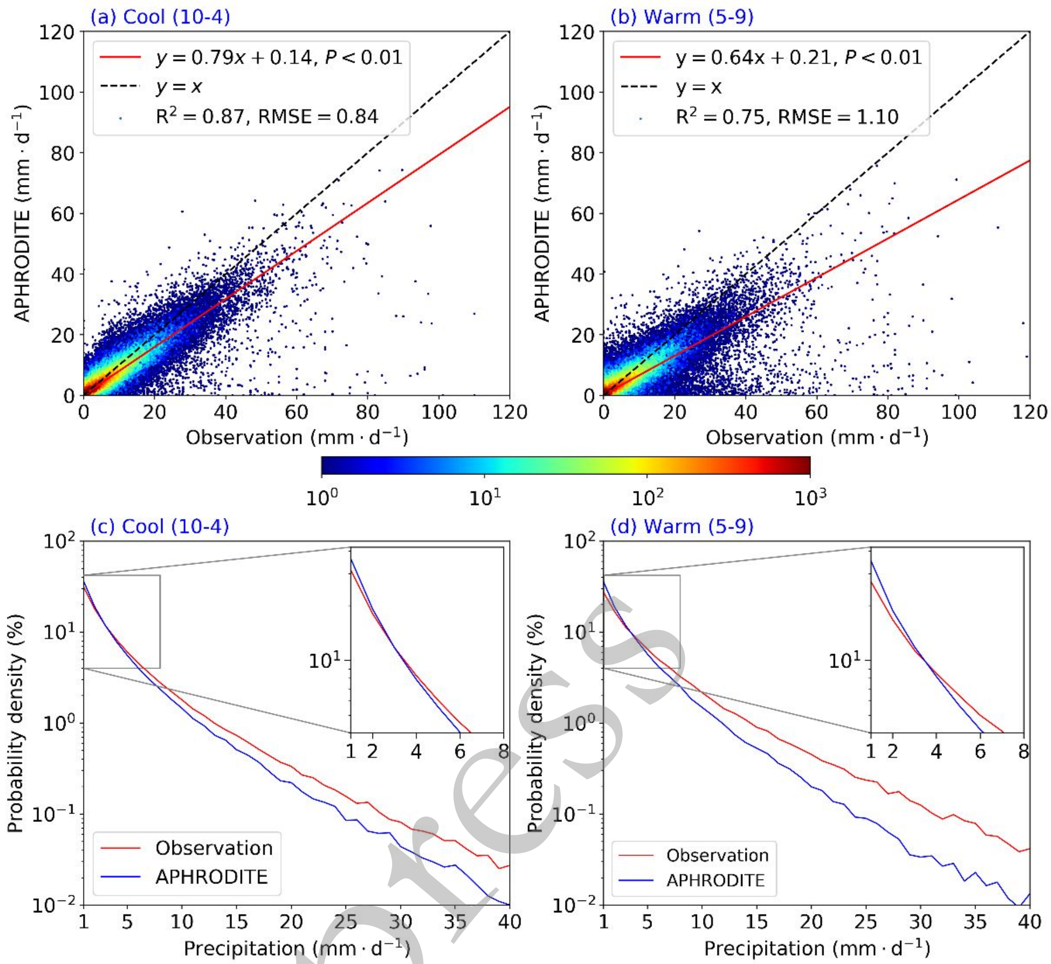

Fig. 7. Density colored scatterplots of precipitation from observations and APHRODITE during the (a) cool and (b) warm seasons. Colors indicate the total numbers and the red line denotes the linear regression between the observation precipitation and the APHRODITE precipitation. PDFs of precipitation for observation (red) and APHRODITE (blue) during the (c) cool and (d) warm season.

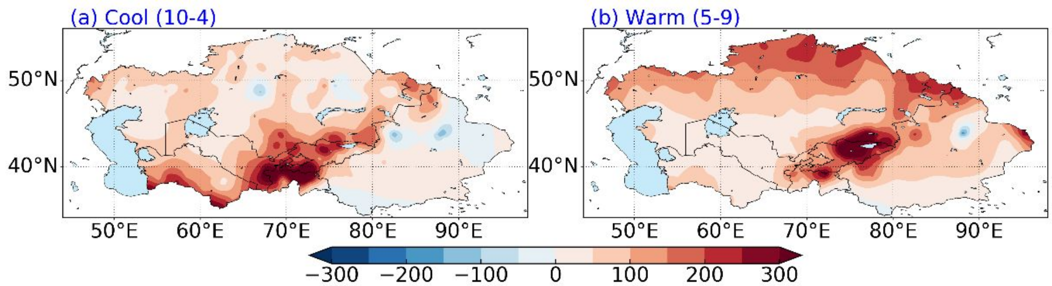

582

583 **Fig. 8.** The spatial distribution of biases in the total number of the wet days (>1 mm d^{-1})

584 between APHRODITE and the observations in Central Asia during (a) the cool season and

585 (b) the warm season during 1961–1990.

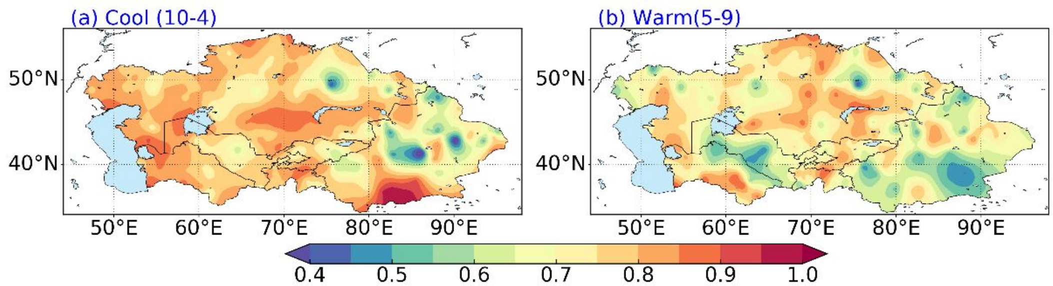

Fig. 9. The spatial distribution of the POD of extreme precipitation derived from APHRODITE in Central Asia during the (a) cool season and (b) warm season.

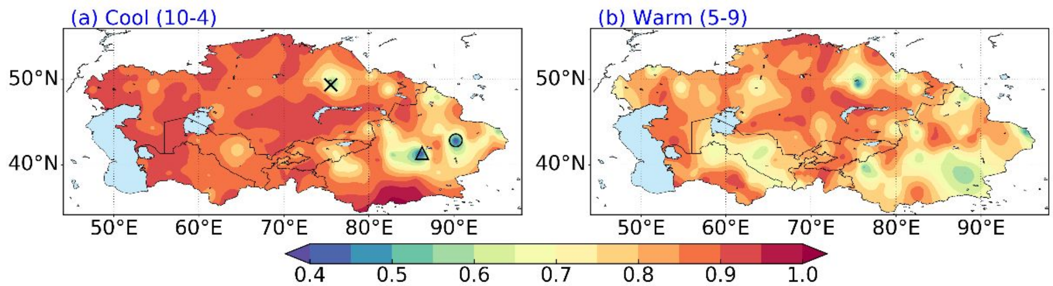

Fig. 10. As in Figure 9, but for EDI. Markers in (a) indicate locations of station No.36335 (cross), No.51581 (circle) and No.51655 (triangle), respectively.

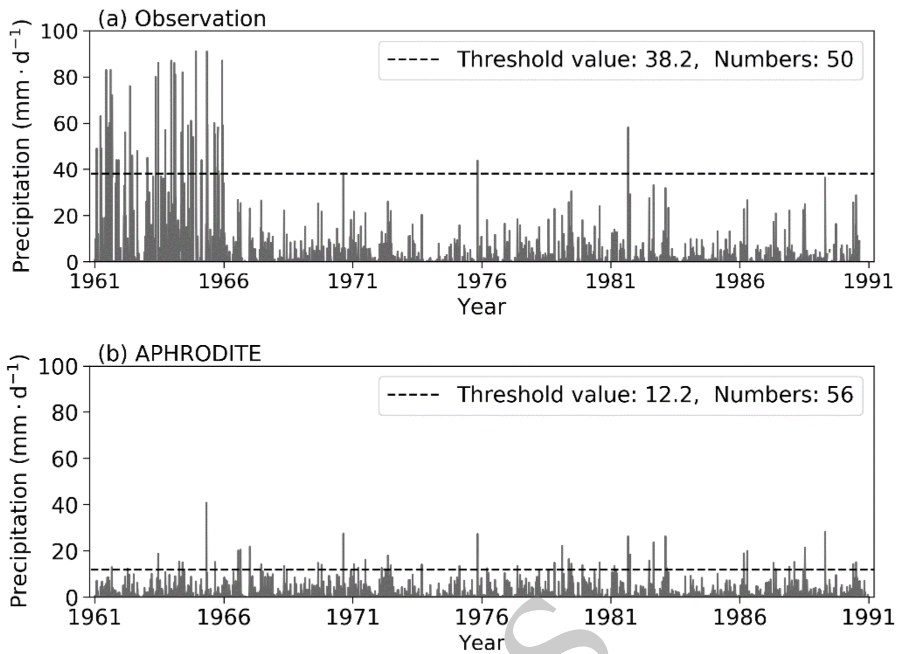

Fig. 11. Time series of daily precipitation for (a) station number 36335 and (b) its nearest grid point in APHRODITE in the warm season during 1961–1990. The dash lines represent the extreme precipitation criterion.

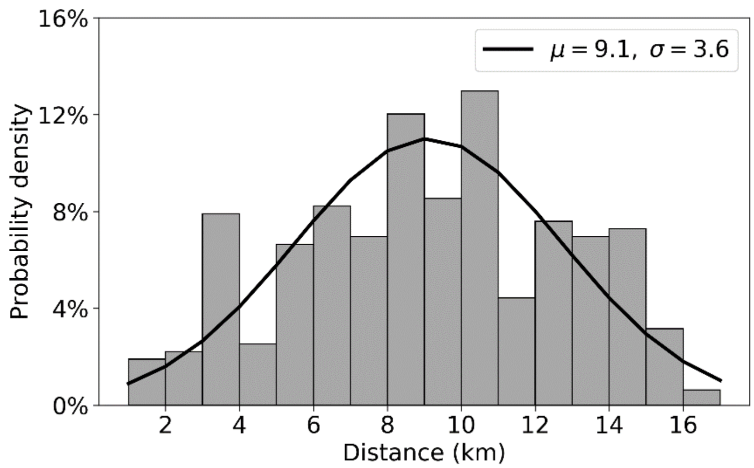

Fig. 12. Histogram of distance between each observation station and its nearest grid point in APHRODITE. The black line indicates the PDFs derived from a normal distribution fitting method.